Role of atomic radius and *d*-states hybridization in the stability of the crystal structure of M_2O_3 (M = Al, Ga, In) oxides

F. P. Sabino* and Luiz Nunes de Oliveira†
Instituto de Física de São Carlos, Universidade de São Paulo, Caixa Postal 369, 13560-970 São Carlos, SP, Brazil

Juarez L. F. Da Silva‡
Instituto de Química de São Carlos, Universidade de São Paulo, Caixa Postal 780, 13560-970 São Carlos, SP, Brazil

(Received 9 July 2014; revised manuscript received 7 September 2014; published 29 October 2014)

We study the stability of the corundum, gallia, and bixbyite structures of Al_2O_3, Ga_2O_3, and In_2O_3 with density functional theory calculations. To artificially control the relative position of the *d* states within the band structure, we add a Hubbard-like on-site Coulomb interaction to the *d* states. We quantitatively show that smaller (larger) atomic radii favor the corundum (bixbyte) structure, which supports empirical models based on the atomic radius ratio between the cation and anions and the spacing-filling condition. Thus, Al_2O_3 and In_2O_3 crystallizes in the corundum and bixbyite structures, which is consistent with experimental observations. The empirical models based on atomic radius and space filling would predict a corundum or bixbyite structure for Ga_2O_3. However, as expected from experimental observations, we find gallia to be the most stable structure for Ga_2O_3. Our results explain why Ga_2O_3 crystallizes in the gallia structures instead of the corundum or bixbyite as follows. The stability of gallia increases as the hybridization of the Ga *d* states with the O 2*s* states grows and the *p*-*d* splitting increases, which is maximized by the presence of fourfold cation sites. The presence of the fourfold cation sites in gallia is a key structural feature that increases its relative stability compared with the corundum and bixbyite structures for Ga_2O_3, which contain only sixfold cation sites, so that the effect of the *d* states is unimportant.

DOI: 10.1103/PhysRevB.90.155206 PACS number(s): 71.15.Mb, 71.15.Nc, 77.84.Bw

I. INTRODUCTION

Transparent conducting oxides (TCO's) constitute a special class of materials that combines high electrical conductivity with approximately 90% visible-light transparency [1]. The TCO's have a wide variety of technological applications, including solar cells [2], light emitting diodes [3], and transparent transistors [4–6]. The high conductivity and transparency of Sn-doped In_2O_3, which can be mainly attributed to the lower conduction-band minimum (CBM) and the optical band gap of about 3.60 eV for In_2O_3[7], is prized in industry, notwithstanding the high cost of the material. Other oxides, such as Ga_2O_3 and Al_2O_3, are also valuable because of their wide gaps that can be exploited in ultraviolet applications and band-gap engineering by the formation of multicompounds with different oxides, e.g., Ga_2O_3-$(ZnO)_n$ [8,9], Al_2O_3-$(ZnO)_n$ [10,11].

In spite of the importance of these three oxides in technological applications, the structural relation among the Al_2O_3, Ga_2O_3, and In_2O_3 oxides remains unclear, even though the three chemical elements, Al, Ga, and In, are neighbors in the same column of the periodic table. The crystal structures of the oxides formed by the three elements are distinct: corundum (rhombohedral, $R\bar{3}c$) for Al_2O_3 [12], gallia (monoclinic, $C2/m$) for Ga_2O_3 [13], and bixbyite (body center cubic, $Ia\bar{3}$) for In_2O_3 [14]. It has been known that the atomic radius plays a crucial role in the atomic structure of oxide systems, but this is insufficient to explain the diversity as discussed below.

Considerations of space filling and of the cationic- to anionic-radius ratios have suggested that oxides with smaller cations (r_c < 0.62–0.69 Å) crystallize in the corundum structure, while cations with medium radius (0.62–0.69 Å < r_c < 0.98–1.00 Å) crystallize in the bixbyite structure, and large cationic radii (r_c > 0.98–1.00 Å) crystallize in the La_2O_3-type structure [15]. Thus, based on the ionic radii of Al (0.50 Å), Ga (0.62 Å), and In (0.81 Å) [16], we would predict a corundum structure for Al_2O_3 and bixbyite for In_2O_3, which is consistent with experimental observations [12,14]. Within the ionic-radius error bars, we would expect Ga_2O_3 to crystallize in either the corundum or bixbyite structures. Neither one of these structures being experimentally observed, we may ask why Ga_2O_3 crystallizes in the gallia structure [13], not in the bixbyite or corundum structures.

Here, we address that question. Our reasoning builds upon the notion that the *d* orbitals of gallium and indium, which are absent in Al, add a new dimension to the problem and undercut arguments solely attentive to the radii. We therefore focus our analysis on the combined influence of the hybridization among the cation and anion states and the radius of the metal atom on the stability of the M_2O_3-oxide (M = Al, Ga, and In) lattice structure. To artificially control the hybridization, we add a Hubbard-like on-site Coulomb interaction U_{eff} to the *d* states, which allows us to push their energy up or down within the band structure, and hence, it affects the hybridization among the *s*-*d* (*s* state derived from the O 2*s* state) and *p*-*d* states. For Ga_2O_3, our results show that the gallia structure is more stable than the bixbyite structure, and that the stability is inextricably linked to the hybridization among the cation *d* states and anion *s* states, which is maximized in fourfold environments. For In_2O_3, by contrast, bixbyite is the most stable structure, because the energetic cost of inserting the

*fernandopsabino@yahoo.com.br
†luizno@usp.br
‡Corresponding author: juarez_dasilva@iqsc.usp.br

large indium atoms in the gallia structure exceeds the gain due to hybridization.

II. THEORETICAL APPROACH AND COMPUTATIONAL DETAILS

A. Total-energy calculations

Our first-principles calculations are based on density-functional theory [17,18] (DFT) within the semilocal Perdew-Burke-Ernzerhof (PBE) exchange-correlation energy functional [19]. As already mentioned, to change the position of the d states within the band structure of the Ga_2O_3 and In_2O_3 oxides and control the s-d and p-d splitting [s and p states derived from the O $2s$ and $2p$ states and d states derived from the $3d$ state (Ga) or $4d$ state (In)], we employ the Hubbard correction proposed by Dudarev *et al.* [20]. Accordingly, we add a Hubbard U, which represents the mean-field approximation to the on-site Coulomb interaction, to the d states. In Dudarev's rotationally invariant approach, only the difference $U_{\text{eff}} = U - J$ between the Coulomb U and the exchange parameter J is physically significant [20]. We let U_{eff} range from $+10$ to -20 eV, to shift the d states up or down relative to their PBE reference energy, and hence we control the relative position of the d states within the band structure and the hybridization of the d states with the O valence states.

Within the DFT+U framework, we have used the all-electron projected augmented wave (PAW) method [21,22] as implemented in the Vienna *Ab-initio* Simulation Package (VASP) [23,24]. We employed the PAW projectors provided within VASP, e.g., O ($2s^2 2p^4$), Al ($3s^2 3p^1$), Ga ($3d^{10} 4s^2 4p^1$), and In ($4d^{10} 5s^2 5p^1$), in which the d states were taken into account to describe the valence of the Ga and In atoms. In addition, to better understand the role of the hybridization between the d states and the O valence states and how it affects the relative stability, we have also carried out calculations without d states in the valence for the Ga and In atoms, i.e., Ga ($4s^2 4p^1$), and In ($5s^2 5p^1$).

To obtain the equilibrium volumes, we minimized the quantum-mechanical stress tensor and atomic forces using a plane-wave cutoff energy of 600 eV, which is required due to the slow convergence of the stress tensor as a function of the number of plane waves. To compute the total energies at the equilibrium volumes, and density of states (DOS), a smaller cutoff energy (450 eV) was employed, which is larger than the maximum cutoff energy suggested for the O PAW projectors (400 eV). For the Brillouin-zone (BZ) integration, we have chosen a **k**-point mesh of $4\times4\times4$ (eight **k** points in the irreducible part of the BZ) for Ga_2O_3 in the bixbyite structure and used the same **k**-point density for all the other bulk systems. For the DOS calculations, we have doubled the **k**-point density and employed a Gaussian smearing of 0.05 eV.

B. Bulk crystal configurations

At room temperature and pressure, the Al_2O_3, Ga_2O_3, and In_2O_3 oxides can be found in the corundum (rhombohedral, $R\bar{3}c$, $Z = 6$) [12], gallia (monoclinic, $C2/m$, $Z = 4$) [13], and bixbyite (cubic, $Ia\bar{3}$, $Z = 8$) [14] structures, respectively, where the crystalline system, space group, and number of formula units, Z, per unit cell are indicated within parentheses. To better understand their relative stability, we have also considered alternative crystal structures for the three oxides, namely, the isostructures of $InFeO_3$ (hexagonal, $P6_3/mmc$, $Z = 2$) [25], La_2O_3 (hexagonal, $P\bar{3}m1$, $Z = 1$) [26], and ϵ-Ga_2O_3 (orthorhombic, $Pna2_1$, $Z = 8$) [27].

In both the bixbyite and corundum structures, only ideal and distorted octahedron motifs are formed, i.e., the cations are surrounded by six oxygen atoms, and hence there is only one cation oxidation state. In contrast, both gallia and ϵ-Ga_2O_3-type structures combine distorted octahedral and tetrahedral motifs with a wide range of coordinations for the oxygen atoms, namely, threefold, fourfold, and fivefold. Although both Ga atoms have different coordination environment, the electron counting rule yields the same oxidation state for the Ga atoms, namely III. The $InFeO_3$-type structure can be described as a sequence of ideal InO_2 octahedral layers separated by trigonal bipyramid FeO layers (Fe is fivefold), which build up the interface between the InO_2 layers. In the La_2O_3-type structure, the cations are surrounded by seven anions. Six of these cation-anion bond lengths are approximately the same, while the seventh oxygen lies farther away. This considered, we take care to select particular crystal structures in which the environment of the cations change from fourfold to sevenfold. Our goal is to identify trends helping to explain the relative stability of the corundum, gallia, and bixbyite structures.

III. RESULTS

All the aforementioned crystal structures were optimized for Al_2O_3, Ga_2O_3, and In_2O_3. The relative stability, structural parameters, and DOS will be discussed below. Unless mentioned, all results include d states in the valence for the Ga and In atoms.

A. Relative stability

The equilibrium PBE ($U_{\text{eff}} = 0.0$ eV) crystal structures are shown in Fig. 1 along with the relative total energies ($\Delta E^i_{\text{tot}} = E^i_{\text{tot}} - E^{\text{bixbyite}}_{\text{tot}}$) per formula unit (f.u.) for all selected configurations, while the PBE lattice parameters are summarized in Table I. For Ga_2O_3 and In_2O_3, we have also calculated ΔE^i_{tot} with the d states frozen in the core. From our definition, $\Delta E^i_{\text{tot}} < 0$ ($\Delta E^i_{\text{tot}} > 0$) implies that the structure i has lower (higher) energy than the bixbyite configuration.

1. PBE results with d states in the valence

As expected from previous DFT calculations [9,28,29], in consistency with experiments [12–14], the lowest-energy PBE structures for Al_2O_3, Ga_2O_3, and In_2O_3 are corundum, gallia, and bixbyite, respectively. The relative total energies are not as large as one might expect. For example, for Al_2O_3, the corundum structure is only 0.15, 0.05, and 0.09 eV per f.u. lower in energy than the bixbyite, gallia, and ϵ-Ga_2O_3-type structures, respectively. Similarly small differences were also obtained for Ga_2O_3. The differences are slightly larger for In_2O_3, however. One would not be surprised, therefore, to see the crystal-structure energy hierarchy change under the influence of the d states, which can be shifted within the band

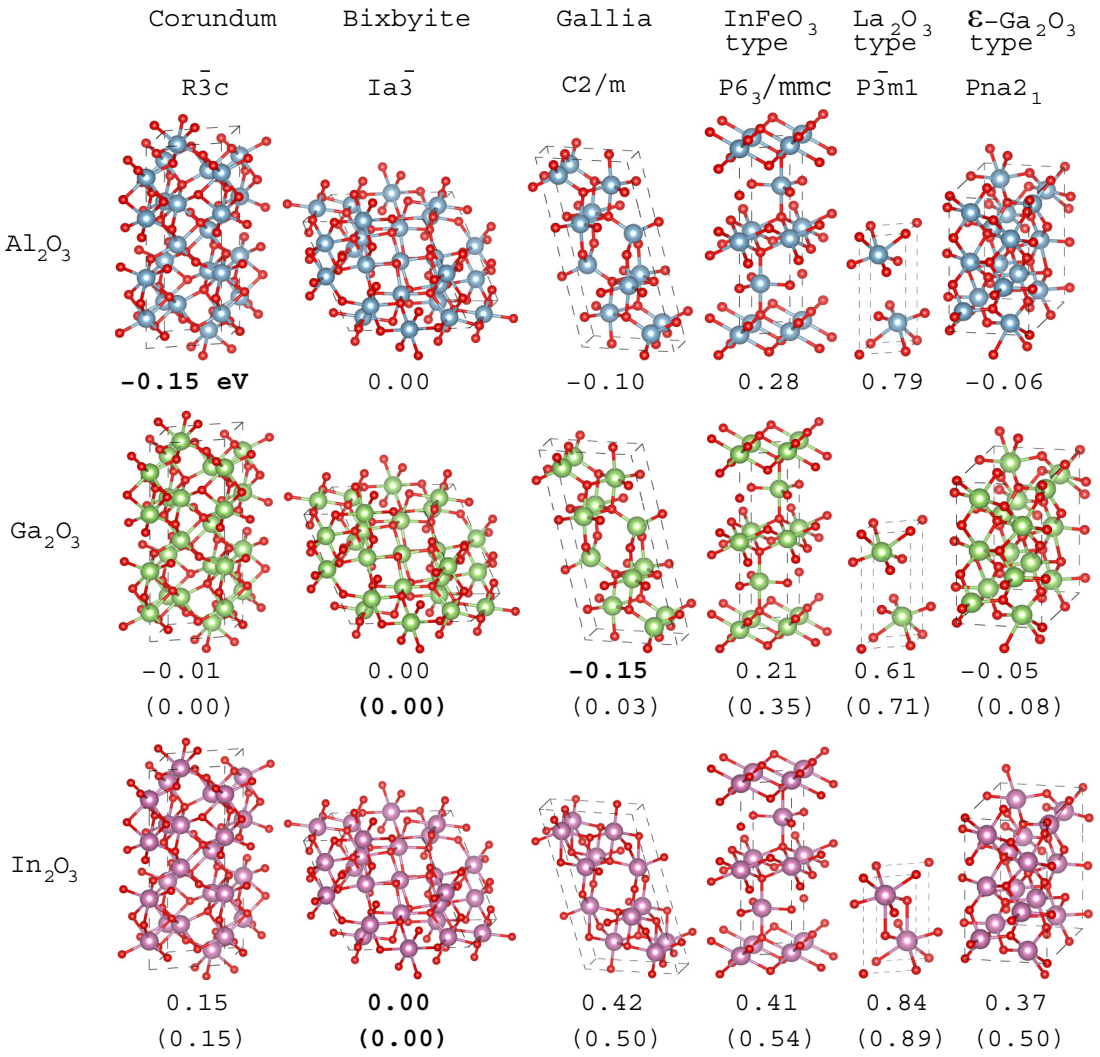

FIG. 1. (Color online) Equilibrium PBE crystal structures for Al_2O_3, Ga_2O_3, and In_2O_3. The space group and the relative total energy per formula unit ($\Delta E^i_{\rm tot} = E^i_{\rm tot} - E^{\rm bixbyite}_{\rm tot}$) are shown above and below the structures, respectively. The numbers in parentheses are the results without *d* states in the valence for the Ga and In atoms. The cation and anion atoms are indicated by the large and small spheres, respectively, and the dashed lines depict the unit cells in the calculations.

structure by adding a Hubbard U to the *d* state or considering the *d* states in the frozen core.

2. *PBE results with d states frozen in the core*

The *d* states are known to play a capital role in systems like GaN and InN [30]. We have found that this is also the case for Ga_2O_3. The hierarchy of relative stabilities for Ga_2O_3 changes when the *d* states are frozen in the core, namely, $\Delta E^i_{\rm tot} > 0$ eV for gallia, $InFeO_3$-, La_2O_3-, and ϵ-Ga_2O_3-type structures, while the corundum and bixbyite structures are degenerate in energy ($\Delta E_{\rm tot} = 0.0$ eV). The gallia, $InFeO_3$- and ϵ-Ga_2O_3-type structures change their relative stability by 0.18, 0.14, and 0.13 eV, respectively, while corundum changes by 0.01 eV. For In_2O_3, there is no analogous change in the relative stability. Notice should be taken, however, that $\Delta E^{\rm Gallia}_{\rm tot}$ increases from 0.42 to 0.52 eV, i.e., the relative stability of In_2O_3 in the gallia structure decreases with the *d* states in the core. Therefore, the main changes occur for Ga_2O_3, in structures that contain fourfold cation sites.

3. *PBE+U results with d states in the valence*

The relative total energy as a function of $U_{\rm eff}$ is shown in Fig. 2. Although gallia, for Ga_2O_3, and bixbyite, for In_2O_3, are the lowest-energy structures over the entire -20.0 eV $\leqslant U_{\rm eff} \leqslant +10.0$ eV range, the relative energies are far from independent of $U_{\rm eff}$. For Ga_2O_3, while the gallia and bixbyite structures are nearly degenerate for $U_{\rm eff} = -20.0$ eV ($\Delta E_{\rm tot} = -10$ meV), the energy separation grows with $U_{\rm eff}$ and reaches $\Delta E_{\rm tot} = 0.43$ eV for $U_{\rm eff} = 10.0$ eV. In fact, for $U_{\rm eff} = 10.0$ eV, corundum and ϵ-Ga_2O_3 lie lower in energy than bixbyite, although higher than gallia. By comparison, the relative energies for In_2O_3 depend more weakly on the Coulomb energy: except for the La_2O_3 structure, $\Delta E_{\rm tot}$ remains nearly constant as $U_{\rm eff}$ grows from -20 to $+10$ eV.

Thus, our results show that the relative stability of the gallia structure compared with the corundum and bixbyite structures for Ga_2O_3 is strongly dependent on the position of the *d* states within the band structure. Therefore, beyond the role played by the relative atomic sizes of the cations and anions, we have

TABLE I. (Color online) Equilibrium lattice parameters a_0, b_0, c_0, β, and resulting volume, effective coordination numbers (ECN) for the Al, Ga, and In atoms, and weighted-average bond lengths d_{av} separating the Al, Ga, and In atoms from the nearest O neighbor for all nonequivalent cation sites. The symbol representing each structure in Figs. 2 and 3 is also shown. The calculated data for the ground-state structures are shown in bold face, and the corresponding experimental values, within parentheses [12–14].

System	Structure	Symbol	a_0 (Å)	b_0 (Å)	c_0 (Å)	β (deg)	Volume/f.u. (Å^3)	ECN	d_{av} (Å)
Al_2O_3	$R\bar{3}c$	●	**4.81**	**4.81**	**13.12**		**43.72**	**5.82**	**1.92**
	$R\bar{3}c$ [12]	●	(4.76)	(4.76)	(12.99)			(5.76)	(1.86)
	$Ia\bar{3}$	■	8.97	8.97	8.97		48.17	5.86, 6.00	1.93, 1.93
	$C2/m$	◆	11.92	2.94	5.67	104.04	48.17	3.99, 5.82	1.78, 1.93
	$P6_3/mmc$	▼	3.04	3.04	11.62		46.44	4.52, 6.00	1.80, 1.99
	$P\bar{3}m1$	▲	2.89	2.89	7.18		51.94	4.25	1.86
	$Pna2_1$	◀	4.88	8.39	9.02		46.20	3.99, 4.99, 5.18, 5.85	1.78, 1.90, 1.92, 2.05
Ga_2O_3	$R\bar{3}c$	○	5.06	5.06	13.63		50.46	5.71	2.01
	$Ia\bar{3}$	□	9.41	9.41	9.41		52.12	5.87, 6.00	2.02, 2.02
	$C2/m$	◇	**12.46**	**3.09**	**5.88**	**103.70**	**54.94**	**3.99**, **5.81**	**1.87**, **2.02**
	$C2/m$ [13]	◇	(12.23)	(3.04)	(5.80)	(103.70)		(3.99), (5.81)	(1.84), (1.98)
	$P6_3/mmc$	▽	3.19	3.19	12.06		53.27	4.59, 6.00	1.89, 2.09
	$P\bar{3}m1$	△	3.03	3.03	7.19		57.18	4.47	1.97
	$Pna2_1$	◁	5.13	8.80	9.42		53.13	3.99, 4.92, 5.20, 5.82	1.87, 1.98, 2.01, 2.13
In_2O_3	$R\bar{3}c$	○	5.58	5.58	14.76		66.33	5.83	2.21
	$Ia\bar{3}$	□	**10.30**	**10.30**	**10.30**		**68.20**	**5.94**, **6.00**	**2.21**, **2.21**
	$Ia\bar{3}$ [14]	□	(10.12)	(10.12)	(10.12)			(5.94), (6.00)	(2.17), (2.19)
	$C2/m$	◇	12.32	3.36	6.91	106.13	68.82	4.47, 5.71	2.14, 2.21
	$P6_3/mmc$	▽	3.56	3.56	12.71		69.81	4.85, 6.01	2.10, 2.28
	$P\bar{3}m1$	△	3.45	3.45	6.30		64.78	4.97	2.20
	$Pna2_1$	◁	5.68	9.64	10.28		70.32	3.99, 5.08, 5.38, 5.83	2.08, 2.18, 2.21, 2.35

identified a second mechanism, associated with the relative position of the Ga d states within the band structure, which accounts for the stability of the gallia structure instead of the expected corundum or bixbyite structures.

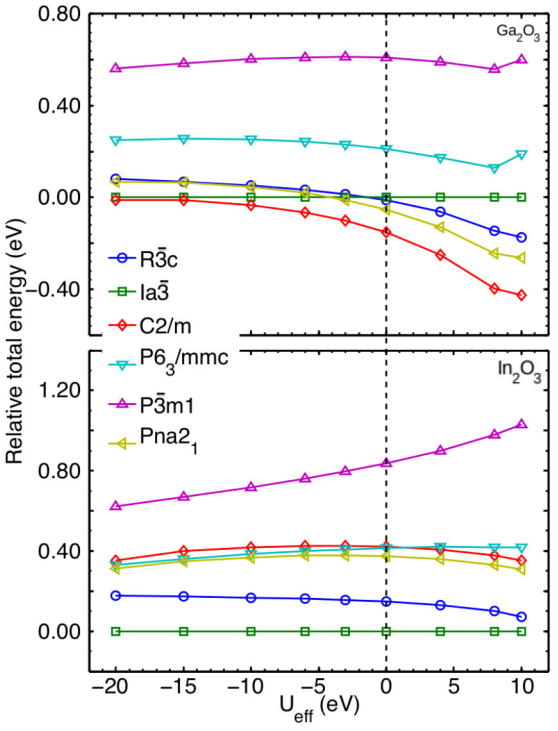

FIG. 2. (Color online) Relative total energy of Ga_2O_3 and In_2O_3 as functions of the effective Hubbard parameter, U_{eff}.

B. Structural properties

The equilibrium PBE parameters are listed in Table I, compared with the experimental results [12–14]. For Al_2O_2 corundum, Ga_2O_3 gallia, and In_2O_3 bixbyite, the lattice constants are overestimated from 1.00% to 1.86%, relative errors that are comparable to the deviations commonly found in DFT-PBE calculations [30,31]. For each system, the crystalline equilibrium volume increases as we move down the periodic table. This is expected, since the ionic radius grows from 0.50 Å for Al, to 0.62 Å for Ga, and 0.81 Å for In [16].

More specific information on the relation between local environment and structural stability can be obtained from the effective coordination concept, which yields the average effective coordination numbers (ECN) and weighted-average bond lengths, d_{av} [32,33]. The results are summarized in Table I for the nonequivalent cationic sites. In the bixbyite structure, there are two nonequivalent cationic sites, namely, an ideal octahedron with ECN = 6, and a distorted octahedron, which increases its distortion for smaller atoms such as Al (ECN = 5.86), while for larger atoms, such as In, the coordination is closer to the ideal value (ECN = 6). For gallia, there are also two nonequivalent sites, namely, fourfold and sixfold. We found that the In atoms in the fourfold sites maximize their coordination, e.g., ECN = 3.99 for Al and Ga atoms, and 4.47 for In, which is expected as large ions tend to maximize their coordination environment. In contrast with gallia and bixbyite,

corundum has only one nonequivalent cationic site, which forms distorted octahedra, i.e., ECN = 5.82, 5.71, and 5.83 for Al, Ga, and In, respectively. Thus, our analysis indicates that In seeks high coordination sites, which is consistent with previous results [29].

From the average bond lengths in Table I, we can estimate the atomic radii of the Al, Ga, and In cations in each structure by $d_{av}/2$, i.e., from the hard-sphere model approximation. We prefer this model to adopting a fixed radius for each element, e.g., the value in Ref. [16], because the O radius varies from coordination site to coordination site. Hence, in the corundum, gallia, and bixbyite structures, the Al, Ga, and In radii are 0.96, 0.97, and 1.11 Å, respectively, which are substantially larger than the ionic radii [16], even if as expected they have the right trend, i.e., the atomic radius increases from Al to In. For the d states frozen in the core, the atomic radius of Ga and In atoms is 0.98 Å (gallia) and 1.11 Å (bixbyite), respectively, i.e., nearly the same with d states in the valence. Thus, the change in the stability of Ga_2O_3 in the gallia structure, Fig. 1, is related to electronic effects, and not to changes in the atomic radius.

The unit cells shrink as U_{eff} grows, and so the atomic radii diminish. The relative total energies as functions of the calculated atomic radius are shown in Fig. 3. While the ○ (□), which represent the corundum (bixbyite) structure for Ga_2O_3 (solid line) and In_2O_3 (dashed line) lie along an approximately continuous line; the solid lines representing Ga_2O_3 for the other structures are separated by marked discontinuities from the dashed curves representing In_2O_3. These results can be explained as follows: (i) The cationic radius plays the chief role in the relative stabilities of corundum and bixbyite. Both structures have only sixfold octahedra cation sites, the relative stability of which is unaffected by the addition of the d states in the valence of the Ga and In atoms. Our calculations with the d states frozen in the core ratifies this inference. (ii) The discontinuities for the gallia and remaining structures can be explained by the hybridization of the cation and O states, which is more effective for lower-coordination cation sites, for gallia Ga_2O_3 in particular. We next turn to the density of states to pinpoint the source of this dependence.

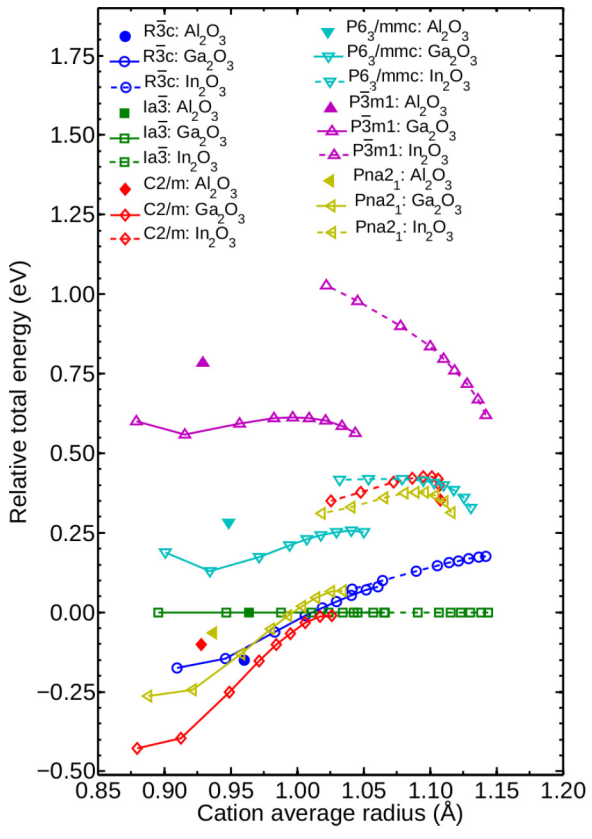

FIG. 3. (Color online) Relative total energy as a function of the cation average radius $d_{av}/2$ for Al, Ga, and In atoms in different crystal structures. The Al_2O_3, Ga_2O_3, and In_2O_3 systems are represented by a lone symbol, a continuous line, and a dashed line respectively.

C. Density of states

Figure 4(a) shows the PBE local densities of states (LDOS) for the corundum, gallia, and bixbyite structures of Al_2O_3, Ga_2O_3, and In_2O_3, respectively. For all systems, the top of the valence band is primarily formed by O delocalized p states, and the bottom of conduction band is formed mainly by the delocalized cationic s states. The Ga and In d states and the O s states derived from O $2s$ states, which are localized, lie at the bottom of the valence band, namely the s band below the d band. The band gaps at the Γ point are 5.86 eV for Al_2O_3, 2.00 eV for Ga_2O_3, and 0.92 eV for In_2O_3. As expected, PBE strongly underestimates the band gaps: the experimental values are 9.25 eV [34], 4.90 eV [35], and 2.90 eV [7], respectively.

Figure 4(b) displays the PBE+U LDOS results for Ga_2O_3 in the gallia structure. As expected, the Hubbard-model Coulomb potential shifts the center of gravity of the d band, and consequently affects the O s and p states. As U_{eff} decreases, the d band is pushed away from the O $2s$ state, towards the O $2p$ states. The solid purple line associated with $U_{eff} = 10$ eV in the top panel shows a small structure at −15 eV, which becomes less pronounced and follows the sharp peak in the bottom panel as U_{eff} is reduced. Likewise, the $U_{eff} = 10$ eV curve in the middle panel shows a small structure around −17 eV that follows the peak in the bottom panel and becomes more salient as U_{eff} is reduced. This shows that the hybridizations between the Ga $3d$ state and the O $2s$ state ($2p$ state) become stronger (weaker) as U_{eff} grows. Our discussion of Fig. 2 having shown that the relative stability of gallia is strongly enhanced as U_{eff} grows, we infer that the hybridization between the Ga $3d$ and the O $2s$ states plays an important role for the stability of the Ga_2O_3 gallia structure.

To verify this reasoning, Fig. 4(c) displays the PBE LDOS for the Ga and O s states, Ga and O p states, and Ga d state in the $C2/m$ structure for Ga_2O_3 calculated with the Ga $3d^{10}4s^24p^1$ the $4s^24p^1$ (d states frozen in the core) PAW projectors. The red line (O for Ga:$3d^{10}4s^24p^1$) displays the small structure discussed in the previous paragraph, but no such feature is identifiable in the blue line (O for Ga:$3d^{10}4s^24p^1$). This confirms that the small asymmetric peak at −13 eV and the narrowing of the more prominent feature around −18 eV in the top panel reflect the hybridization between the Ga $3d$ and the O $2s$ states. Without the $3d$ orbitals among the valence states, the hybridization vanishes, and we

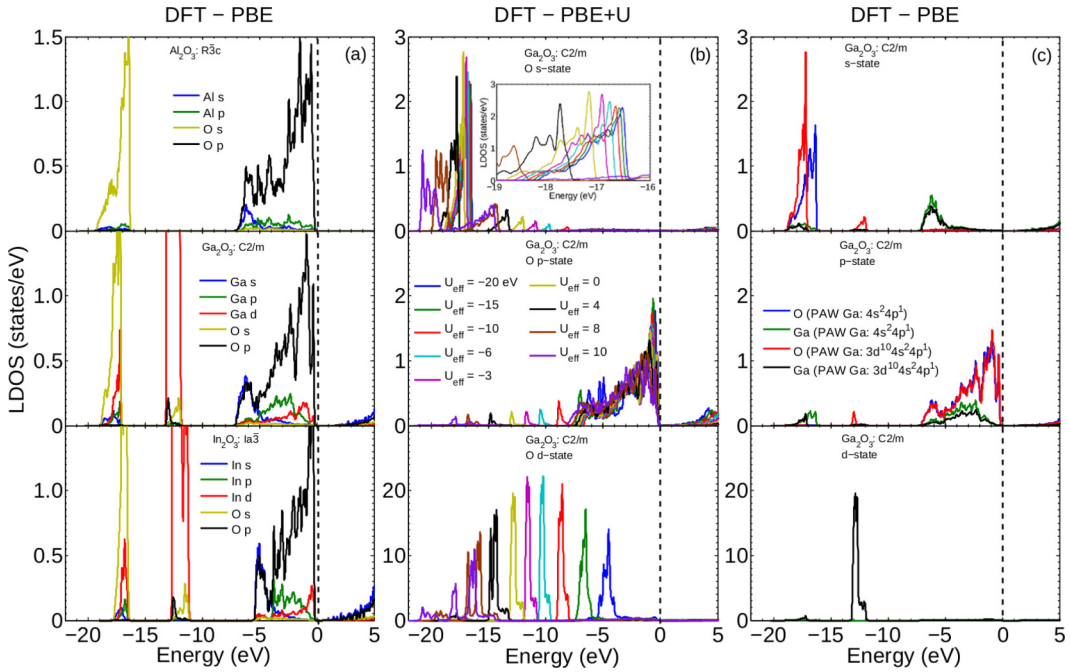

FIG. 4. (Color online) (a) Local densities of states for the corundum, gallia, and bixbyite structures of Al_2O_3, Ga_2O_3, and In_2O_3 respectively. (b) Local densities of states for O-s, O-p, and Ga-d for Ga_2O_3 in the $C2/m$ structure, for the indicated U_{eff}. (c) Local densities of states for O-s and Ga-s, O-p and Ga-p, Ga-d for Ga_2O_3 in the $C2/m$ (gallia) structure with different PAW projectors for Ga: Ga ($3d^{10}4s^24p^1$) and Ga ($4s^24p^1$). The dashed vertical line marks the Fermi level.

expect the bixbyite structure to become more stable, which is confirmed by our calculations, Fig. 1.

Were the Ga 3d and O 2s bands partially filled, substantial energy gain would result from the hybridization-induced depression (uplift) of the bonding (antibonding) levels, a gain chiefly due to optimization of the kinetic plus potential energies of the system. Since the 3d and 2s bands are filled, the hybridization only affects the interaction, i.e., Hartree, exchange, and correlation energies, via redistribution of the ground-state density. The resulting energy gain is relatively small, however, it changes the relative stability of the gallia structure given that the gallia structure is only 0.18 eV/f.u. higher in energy than the bixbyite structure.

The LDOS for In_2O_3, not shown in the figure, shows analogous features. The hybridization between the O 2s and the In 4d states shifts down the relative total energy ΔE_{tot} of gallia-structured In_2O_3. The reduction is however insufficient to offset the energy cost of positioning indium atoms at the low-coordination sites of the gallia structure. Already discussed in Sec. III B, this cost accounts for the gap separating the dashed line through the ◊ from the solid line through the same symbol in Fig. 3 and, therefore, accounts for the stability of the bixbyite structure.

IV. CONCLUSIONS

We have studied the stability of the corundum, gallia, and bixbyite structures of Al_2O_3, Ga_2O_3, and In_2O_3 with DFT calculations. To artificially control the relative position of the d states within the band structure of the Ga_2O_3 and In_2O_3 oxides, we have added a Hubbard-like on-site Coulomb interaction, U_{eff}, to the d states, which also affects the equilibrium lattice parameters. We have quantitatively shown that smaller (larger) atomic radii favor the corundum (bixbyte) structure, which supports empirical models based on the atomic-radius ratio between the cation and anions and the spacing-filling condition. Thus, Al_2O_3 and In_2O_3 crystallizes in the corundum and bixbyite structures, which is consistent with experimental observations.

The empirical models based on atomic radius and space filling would predict a corundum or bixbyite structure for Ga_2O_3. However, in consistency with experiment, we have found gallia to be the most stable structure for Ga_2O_3. Based on calculations without d states in the valence and on changes of the relative position of the d states within the band structure, we have come to the following explanation of why Ga_2O_3 crystallizes in the gallia structures instead of the corundum or bixbyite. The stability of gallia increases as the hybridization between the Ga d and the O 2s states grows, while the p-d splitting increases, which is maximized in the presence of fourfold cation sites. Therefore, the presence of the fourfold cation sites in gallia is a key structural feature that increases its stability relative to the corundum and bixbyite structures for Ga_2O_3, in which there are only sixfold cation sites.

ACKNOWLEDGMENTS

This research was supported by the CNPq (Grants No. 403142/2012-1 and No. 409921/2013-0), CAPES, and FAPESP (Grant No. 2013/21045-2). The infrastructure provided to our computer cluster by the São Carlos Center of Informatics, University of São Paulo, is gratefully acknowledged.

[1] K. Nomura, H. Ohta, K. Ueda, T. Kamiya, M. Hirano, and H. Hosono, Science **300**, 1269 (2003).

[2] A. S. Gonçalves, M. R. Davalos, N. Masaki, S. Yanagida, A. Morandeira, J. R. Durrant, J. N. Freitas, and A. F. Nogueira, Dalton Trans., 1487 (2008).

[3] J. J. Berry, D. S. Ginley, and P. E. Burrows, Appl. Phys. Lett. **92**, 193304 (2008).

[4] R. E. Presley, D. Hong, H. Q. Chiang, C. M. Hung, R. L. Hoffman, and J. F. Wager, Solid-State Electron. **50**, 500 (2006).

[5] H.-H. Hsieh and C.-C. Wu, Appl. Phys. Lett. **91**, 013502 (2007).

[6] D.-H. Cho, S. Yang, C. Byun, J. Shin, M. K. Ryu, S.-H. K. Park, C.-S. Hwang, S. M. Chung, W.-S. Cheong, S. M. Yoon, and H.-Y. Chu, Appl. Phys. Lett. **93**, 142111 (2008).

[7] A. Walsh, J. L. F. Da Silva, S.-H. Wei, C. Korber, A. Klein, L. F. J. Piper, A. DeMasi, K. E. Smith, G. Panaccione, P. Torelli, D. J. Payne, A. Bourlange, and R. G. Egdell, Phys. Rev. Lett. **100**, 167402 (2008).

[8] Y. Michiue, N. Kimizuka, and Y. Kanke, Acta Crystallogr., Sect. B: Struct. Sci. **64**, 521 (2008).

[9] J. L. F. Da Silva, A. Walsh, and S.-H. Wei, Phys. Rev. B **80**, 214118 (2009).

[10] S. Yoshioka, F. Oba, R. Huang, I. Tanaka, T. Mizoguchi, and T. Yamamoto, J. Appl. Phys. **103**, 014309 (2008).

[11] K. Rijpstra, S. Cottenier, M. Waroquier, and V. V. Speybroeck, CrystEngComm **15**, 10440 (2013).

[12] P. Thompson, D. E. Cox, and J. B. Hastings, J. Appl. Crystallogr. **20**, 79 (1987).

[13] S. Geller, J. Chem. Phys. **33**, 676 (1960).

[14] M. Marezio, Acta Crystallogr. **20**, 723 (1966).

[15] F. Hanic, M. Hartmanová, G. G. Knab, A. A. Ursovskaya, and K. S. Bagdasarov, Acta. Crystallogr., Sect. B: Struct. Sci. **40**, 76 (1984).

[16] C. Kittel, *Introduction to Solid State Physics, 7th ed.* (John Wiley & Sons, New York, 1996).

[17] P. Hohenberg and W. Kohn, Phys. Rev. **136**, B864 (1964).

[18] W. Kohn and L. J. Sham, Phys. Rev. **140**, A1133 (1965).

[19] J. P. Perdew, K. Burke, and M. Ernzerhof, Phys. Rev. Lett. **77**, 3865 (1996).

[20] S. L. Dudarev, G. A. Botton, S. Y. Savrasov, C. J. Humphreys, and A. P. Sutton, Phys. Rev. B **57**, 1505 (1998).

[21] P. E. Blöchl, Phys. Rev. B **50**, 17953 (1994).

[22] G. Kresse and D. Joubert, Phys. Rev. B **59**, 1758 (1999).

[23] G. Kresse and J. Hafner, Phys. Rev. B **48**, 13115 (1993).

[24] G. Kresse and J. Furthmüller, Phys. Rev. B **54**, 11169 (1996).

[25] D. M. Giaquinta, W. M. Davis, and H.-C. zur Loye, Acta Crystallogr., Sect. C: Cryst. Struct. Commun. **50**, 5 (1994).

[26] R. Wyckoff, *Crystal Structures* (Wiley, New York, 1963), Vol. 2 .

[27] K. Matsuzaki, H. Yanagi, T. Kamiya, H. Hiramatsu, K. Nomura, M. Hirano, and H. Hosono, Appl. Phys. Lett. **88**, 092106 (2006).

[28] C. Sevik and C. Bulutay, J. Mater. Sci. **42**, 6555 (2007).

[29] J. L. F. Da Silva, Y. Yan, and S.-H. Wei, Phys. Rev. Lett. **100**, 255501 (2008).

[30] M. Fuchs, J. L. F. Da Silva, C. Stampfl, J. Neugebauer, and M. Scheffler, Phys. Rev. B **65**, 245212 (2002).

[31] P. Haas, F. Tran, and P. Blaha, Phys. Rev. B **79**, 085104 (2009).

[32] R. Hoppe, Z. Kristallogr. **150**, 23 (1979).

[33] J. L. F. Da Silva, J. Appl. Phys. **109**, 023502 (2011).

[34] T. Tomika, Y. Ganaha, T. Shikenbaru, T. Futemma, M. Yuri, Y. Aiura, S. Sato, H. Futukani, H. Kato, T. Miyahara, A. Yonesu, and J. Tamashiro, J. Phys. Soc. Jpn. **62**, 573 (1993).

[35] M. Orita, H. Ohta, M. Hirano, and H. Hosono, Appl. Phys. Lett. **77**, 4166 (2000).